



Long-read single-cell RNA sequencing enables the study of cancer subclone-specific genotypes and phenotypes in chronic lymphocytic leukemia

Gage S. Black, Xiaomeng Huang, Yi Qiao, et al.

Genome Res. 2025 35: 686-697 originally published online February 18, 2025
Access the most recent version at doi:[10.1101/gr.279049.124](https://doi.org/10.1101/gr.279049.124)

References This article cites 46 articles, 8 of which can be accessed free at:
<http://genome.cshlp.org/content/35/4/686.full.html#ref-list-1>

Creative Commons License This article is distributed exclusively by Cold Spring Harbor Laboratory Press for the first six months after the full-issue publication date (see <https://genome.cshlp.org/site/misc/terms.xhtml>). After six months, it is available under a Creative Commons License (Attribution-NonCommercial 4.0 International), as described at <http://creativecommons.org/licenses/by-nc/4.0/>.

Email Alerting Service Receive free email alerts when new articles cite this article - sign up in the box at the top right corner of the article or [click here](#).

To subscribe to *Genome Research* go to:
<https://genome.cshlp.org/subscriptions>

Long-read single-cell RNA sequencing enables the study of cancer subclone-specific genotypes and phenotypes in chronic lymphocytic leukemia

Gage S. Black,¹ Xiaomeng Huang,¹ Yi Qiao,¹ Philip Moos,² Deepa Sampath,³ Deborah M. Stephens,⁴ Jennifer A. Woyach,^{5,6} and Gabor T. Marth^{1,6}

¹Department of Human Genetics, ²Department of Pharmacology and Toxicology, University of Utah, Salt Lake City, Utah 84112, USA; ³Department of Hematopoietic Biology and Malignancy, The University of Texas MD Anderson Cancer Center, Houston, Texas 77054, USA; ⁴Division of Hematology, University of North Carolina, Chapel Hill, North Carolina 27599, USA; ⁵The Ohio State University Comprehensive Cancer Center, Columbus, Ohio 43210, USA

Bruton tyrosine kinase (BTK) inhibitors are effective for the treatment of chronic lymphocytic leukemia (CLL) due to BTK's role in B cell survival and proliferation. Treatment resistance is most commonly caused by the emergence of the hallmark *BTK*^{C481S} mutation that inhibits drug binding. In this study, we aimed to investigate cancer subclones harboring a *BTK*^{C481S} mutation and identify cells with co-occurring CLL driver mutations. In addition, we sought to determine whether *BTK*-mutated subclones exhibit distinct transcriptomic behavior when compared to other cancer subclones. To achieve these goals, we use scBayes, which integrates bulk DNA sequencing and single-cell RNA sequencing (scRNA-seq) data to genotype individual cells for subclone-defining mutations. Although the most common approach for scRNA-seq includes short-read sequencing, transcript coverage is limited due to the vast majority of the reads being concentrated at the priming end of the transcript. Here, we utilized MAS-seq, a long-read scRNA-seq technology, to substantially increase transcript coverage and expand the set of informative mutations to link cells to cancer subclones in six CLL patients who acquired *BTK*^{C481S} mutations during BTK inhibitor treatment. In two patients who developed two independent *BTK*-mutated subclones, we find that most *BTK*-mutated cells have an additional CLL driver gene mutation. When examining subclone-specific gene expression, we find that in one patient, *BTK*-mutated subclones are transcriptionally distinct from the rest of the malignant B cell population with an overexpression of CLL-relevant genes.

[Supplemental material is available for this article.]

Chronic lymphocytic leukemia (CLL) is the most prevalent subtype of leukemia in adults, affecting ~200,000 individuals in the United States, and is characterized by an overaccumulation of dysfunctional B cells (Byrd et al. 2004; Kipps et al. 2017). B cell receptor (BCR) signaling is crucial for cell survival and proliferation, becoming a prime target for therapeutic intervention (Burger and Chiorazzi 2013). The inhibition of Bruton tyrosine kinase (BTK), a kinase necessary for proper BCR signaling, has proven to be an effective treatment for most patients (Petro et al. 2000; Herman et al. 2011; Byrd et al. 2013; Pal Singh et al. 2018). However, secondary resistance to treatment develops in ~20% of patients over time, leading to poor clinical outcomes, including shorter survival (Nakhoda et al. 2023). The *BTK*^{C481S} mutation is the most common cause of BTK inhibitor resistance (up to 80% of relapses). This mutation confers drug resistance by impairing the binding of the drug to CLL cancer cells, transforming the normal covalent BTK inhibitor binding to a noncovalent bond (Woyach et al. 2017; Sedlarikova et al. 2020). The evolution of mutations in additional CLL driver genes has also been shown to contribute to treatment resistance (Komarova et al. 2014; Landau et al. 2015; Burger et al. 2016). Our present study aims to investigate whether the presence of additional CLL driver mutations in

cancer subclones harboring a *BTK*^{C481S} mutation accelerates subclone expansion and whether *BTK*-mutated subclones exhibit distinct transcriptomic behavior when compared to other cancer subclones.

Previously, we have demonstrated the ability to use bulk DNA sequencing to deconvolute cancer subclone structures (Qiao et al. 2014; Brady et al. 2017; Than et al. 2018; Huang et al. 2021; Black et al. 2022), as well as using single-cell RNA sequencing (scRNA-seq) data to genotype individual cells and study subclone-specific transcriptomic behavior using scBayes (Qiao et al. 2024). We use whole-exome sequencing (WES) or whole-genome sequencing of tumor/normal pairs to identify somatic mutations and reconstruct the subclone structure of the tumor as well as its evolution across tumor progression. Individual cells from the scRNA-seq data are assigned to genomic subclones based on the presence or absence of subclone-defining mutations. By combining subclone identity with single-cell gene expression information, this approach enables a subclone-specific gene expression analysis.

Until recently, scRNA-seq has been carried out almost exclusively with short-read sequencing technologies. A disadvantage of traditional short-read scRNA-seq is the 5' or 3' bias, where the vast majority of the reads are concentrated at the 5' or 3' ends of

***These authors contributed equally to this work.**

Corresponding author: gmarth@genetics.utah.edu

Article published online before print. Article, supplemental material, and publication date are at <https://www.genome.org/cgi/doi/10.1101/gr.279049.124>.

© 2025 Black et al. This article is distributed exclusively by Cold Spring Harbor Laboratory Press for the first six months after the full-issue publication date (see <https://genome.cshlp.org/site/misc/terms.xhtml>). After six months, it is available under a Creative Commons License (Attribution-NonCommercial 4.0 International), as described at <http://creativecommons.org/licenses/by-nc/4.0/>.

the transcript (Ziegenhain et al. 2017). This bias limits our ability to determine the cell's genotype at the sites of somatic tumor mutations farther, i.e., at greater than sequencing read length distances, from the priming site. Long-read scRNA-seq provides a promising alternative, as it can improve coverage across the length of the transcript. MAS-seq (now PacBio Kinnex), a long-read scRNA-seq solution by Pacific Biosciences (PacBio), is a ready-to-use kit that concatenates cDNAs generated from the 10x Genomics Chromium platform to create long composite molecules that can be sequenced with over 99.9% accuracy via HiFi sequencing (Wenger et al. 2019; Al'Khafaji et al. 2023). We hypothesized that the highly accurate full-transcript coverage afforded by MAS-seq would yield improved coverage of somatic mutations falling outside the standard short-read length distance of priming sites, thus enabling enhanced single-cell genotyping and subclone assignment.

In a recent study, we investigated subclonal evolution using WES in 38 patients with CLL treated with a BTK inhibitor (Supplemental Table S1; Black et al. 2022). We found that the evolution of subclones containing mutations in CLL driver genes within the first 2 years of treatment had a significant association with eventual relapse. Among these patients, we identified six who developed at least one subclone harboring a *BTK*^{C481S} resistance mutation. Here, we performed long-read scRNA-seq with MAS-seq on samples from these six patients taken before BTK inhibitor treatment and at the time of relapse to use in conjunction with the WES data to study the co-occurrence of *BTK*^{C481S} and additional CLL driver mutations, as well as *BTK*-mutant subclonal phenotypes.

Results

Long-read sequencing with MAS-seq expands transcript and variant coverage

We generated long-read scRNA-seq data for the pretreatment and relapse samples from six CLL patients who developed *BTK*^{C481S} mutations during BTK inhibitor treatment. Cell isolation was performed using the 10x Genomics Chromium 3' Single Cell Kit, followed by cDNA concatenation and HiFi sequencing with PacBio's MAS-seq technology. Four samples were sequenced on the Sequel II system, while eight samples were sequenced on the Revio system. When comparing the number of reads produced by the two sequencing instruments, we find that the Revio produced ~4× the number of reads per sample (Fig. 1A). Samples sequenced on the Sequel II produced an average of 3363 reads per cell, with 4251 cells per sample (Table 1). In contrast, samples sequenced on the Revio produced an average of 9283 reads per cell, with 6239 cells per sample. The read length in the Revio samples (~910 bp) was shorter than in the Sequel II samples (~1100 bp), de-

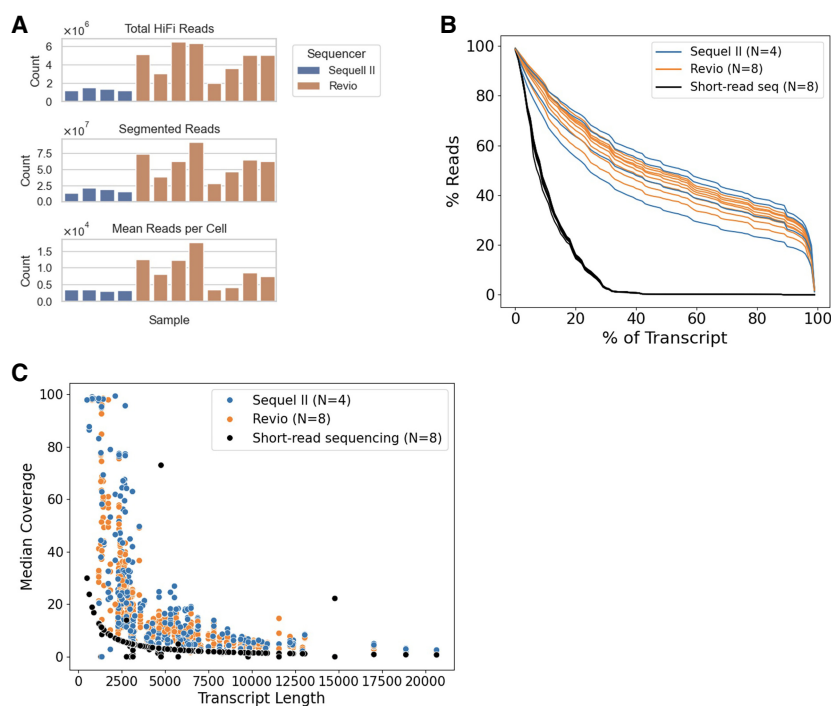


Figure 1. Long-read scRNA-seq metrics. (A) Comparison of the total number of HiFi reads, the total number of segmented reads, and the mean reads per cell for each sample, colored by the sequencer used. (B) The canonical transcript coverage for each read aligning to a given gene is calculated for all protein-coding genes with at least one read aligned to it. The percentage of reads covering X% of the given transcript is plotted for each sample and colored by the sequencer used for the sample. Eight short-read samples are included in black for comparison. (C) Comparison of the median coverage from each sample for the 112 CLL driver genes included in this study. Genes are sorted along the x-axis by the length of the canonical transcript. Each dot represents the coverage of the given gene for a sample, colored by the technology used to sequence the sample.

spite the improvement in the number of reads. All samples across both platforms maintained a high median base quality, consistently at or above Q30. The increase in reads per cell in the Revio samples enhances analysis by providing more informative reads to identify subclone-relevant mutations and quantify gene expression. These outcomes highlight Revio's superior data generation capabilities, offering a more cost-effective long-read sequencing solution.

To examine the transcript coverage afforded by reads generated from MAS-seq, we selected the Ensembl canonical transcripts for all protein-coding genes and calculated the percentage of transcript coverage provided by each read mapping to the given gene (Fig. 1B). In addition, we calculated this same coverage within pretreatment and relapse samples from four patients (within our original 38-patient cohort but not among the six patients in the present study) that were sequenced using short-read scRNA-seq. We find comparable transcript coverage across all samples sequenced with MAS-seq, with 50% of reads covering at least 41.3% of the transcript length and 32.5% of reads covering >80% of the canonical transcript on average. In comparison, we found that the short-read sequencing samples had 50% of reads covering at least 9.1% of the transcript length and only 0.1% of reads covering >80% of the canonical transcript on average. When comparing the median coverage of the canonical transcript of the 112 CLL genes across technologies, we find that the MAS-seq samples had an increase in the number of genes with coverage, as well as in the median coverage across reads (Fig. 1C). Full-transcript

Table 1. Long-read scRNA-seq metrics for each sample across the six patients

Patient	Time point	Sequencer	Cells recovered	Total HiFi reads	Average HiFi read length	Average HiFi read quality	Segmented reads	Segmented reads after barcode correction and UMI deduplication	Average segmented read length	Average reads per cell	Median UMIs per cell	Median genes per cell	Median transcripts per cell
1	Pretreatment	Revio	4384	6,459,939	10,397	30	62,282,311	34,303,737	897	12,300	7001	1107	1317
1	Relapse	Revio	4527	6,305,954	13,674	30	92,245,332	41,177,852	885	17,610	8110	1130	1360
2	Pretreatment	Revio	5357	5,093,438	14,308	30	73,572,836	46,692,179	930	12,539	8038	1259	1540
2	Relapse	Revio	4466	3,046,815	13,338	31	38,840,774	30,954,010	934	8245	5709	897	1070
3	Pretreatment	Sequel II	3025	1,149,291	15,027	32	12,656,112	7,629,323	1158	3490	1866	294	522
3	Relapse	Sequel II	4702	1,518,018	16,691	31	21,029,102	9,086,104	1098	3566	1704	309	344
4	Pretreatment	Sequel II	5337	1,354,734	16,696	32	18,975,741	13,045,554	1104	3147	2235	535	590
4	Relapse	Sequel II	3940	1,149,151	15,178	32	15,146,244	9,103,200	1053	3250	2011	423	472
5	Pretreatment	Revio	7288	1,983,307	13,978	30	27,877,526	21,872,099	907	3473	2302	412	460
5	Relapse	Revio	9372	3,609,493	10,797	30	45,847,606	32,198,895	725	4140	2799	407	468
6	Pretreatment	Revio	7089	5,007,964	12,584	30	64,251,998	49,524,406	845	8504	5801	818	964
6	Relapse	Revio	7429	5,043,744	11,948	30	62,739,550	46,399,766	804	7449	5001	608	702

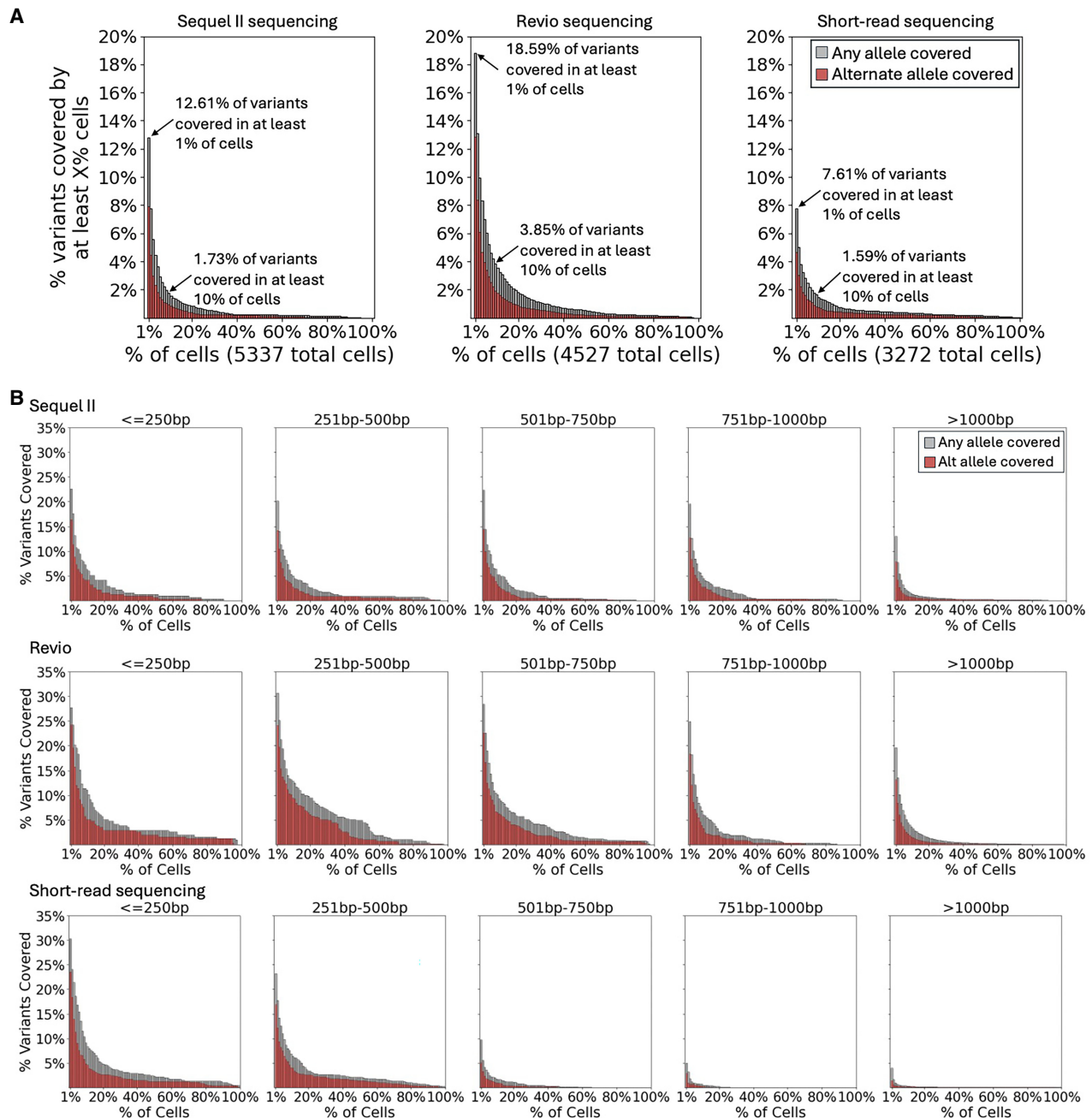


Figure 2. The variant coverage provided by each scRNA-seq technology. (A) The overall variant coverage provided by the Sequel II and Revio compared to Illumina short reads. The percentage of cells covering each heterozygous germline variant in the patient's WES data is used to determine the percent of variants covered by at least X% of cells. (B) The variant coverage is binned by the variant's distance from the priming site, as indicated above each plot (bp = base pairs).

read coverage was limited, as the median transcript length of the 112 CLL genes is 4642 bp. These comparisons illustrate that although full transcript coverage is not always obtained, MAS-seq provides a significant increase in transcript coverage across reads.

To determine our ability to identify multiple mutations within a given cell, we selected heterozygous germline variants from each sample and calculated the percentage of variants with coverage in each cell (Supplemental Fig. 1). Figure 2A illustrates these coverage metrics by comparing the sample with the best coverage

from the Sequel II, Revio, and short-read sequencing technologies. We found that samples sequenced using HiFi sequencing on the Sequel II machine had a 5% increase in variant coverage compared to those sequenced on the short-read sequencer, whereas samples sequenced on the Revio machine showed an 11% increase in variant coverage (Table 2). Furthermore, we characterized each heterozygous germline variant by its distance from the priming end of the transcript to determine the impact of this distance on variant coverage (Fig. 2B; Supplemental Fig. 2). Samples sequenced

Table 2. Summary of germline heterozygous variant coverage provided by each scRNA-seq technology

Sample	Sequencing technology	Number of reads	Number of variants called	% Variants covered by 1% or more cells	% Variants covered by 10% or more cells	% Variants present in scRNA-seq
Patient 3, Pretreatment	Sequel II	13,045,554	13,403	12.61	1.73	43.58
Patient 1, Posttreatment	Revio	41,177,852	13,709	18.59	3.85	50.12
Short-read 1	Short read	713,605,274	12,954	7.61	1.59	33.08

Read counts come from segmented reads after barcode correction and UMI deduplication for HiFi sequencing and only reads that were mapped to the genome. The percentage of germline heterozygous variants identified with WES detected in each scRNA-seq is also shown.

with MAS-seq on either the Revio or Sequel II show variant coverage across all positions in the transcript, with only minor bias for the priming end of the transcript. In contrast, the short-read sequencing shows a high bias in variant coverage for those that are <500 bp from the priming site. These results indicate that MAS-seq provides increased variant coverage per cell compared to short-read sequencing and that this coverage can be seen throughout the entire transcript. The increased, uniform coverage afforded by MAS-seq improves our ability to genotype cells at multiple subclone-defining somatic mutation sites in a single cell, enhancing the quality of cell assignments to cancer subclones.

We assessed the concordance between WES and MAS-seq by comparing the variant allele frequencies (VAFs) produced by the two methods for each patient's somatic mutations. The VAFs of the somatic mutations identified in both data sets show a medium correlation, with a correlation coefficient of 0.4 and an R^2 value of 0.16 when comparing the VAF of all variants across all patients (Supplemental Fig. 3). The observed correlation, although moderate, highlights several important technical and biological differences between the two sequencing approaches. One primary factor contributing to the lack of a stronger correlation is allelic dropout in MAS-seq data, where certain alleles may not be detected due to the stochastic nature of scRNA-seq. Additionally, the lack of expression of some genes in the MAS-seq data, which are captured in the genomic DNA of WES, further exacerbates these differences.

Full transcript coverage allows for the identification and visualization of single-cell genotypes

We have recently published a novel computational method, scBayes, to study cancer subclone-specific expression phenotypes by combining scRNA-seq and bulk DNA sequencing-based subclone structures (Fig. 3A; Qiao et al. 2024). This approach enables genotype inference for mutations lacking sequencing coverage when genotypes are present for other subclone-specific mutations within the same subclone. The cancer subclone structures of the six patients in this study have been extensively characterized in our previous work (Black et al. 2022), allowing us to apply scBayes and assign each cell to a clone of origin (Supplemental Fig. 4). Briefly, scBayes genotypes each cell by examining the presence of subclone-defining somatic mutations (as discovered from bulk

DNA sequencing data, Fig. 3B, y -axis) in the scRNA-seq reads of the cell (Fig. 3B, x -axis) and uses a Bayesian probabilistic framework to identify the most likely clone of origin (Fig. 3B, x -axis color bars) for the cell. Using this method, we were able to confidently assign up to 20% of cells to a predetermined subclone. We use a scatterplot-like visualization (Fig. 3B) to illustrate the cell genotypes for each variant of each cell, showing whether the mutant allele was observed (red), if only the reference allele was observed (green), or if there was no read coverage for the variant (white). Once cells are assigned, those of the same subclone can be grouped together and compared to cells of other subclones for subclone-specific gene expression analysis. Long-read scRNA-seq is particularly suitable for such an approach as it maximizes the likelihood that a somatic mutation is covered by sequencing.

Long-read scRNA-seq enables confirmation or refinement of subclone structures

To determine whether the subclone structures previously identified through WES were corroborated by the long-read scRNA-seq data, we analyzed the structure of each patient at a single-cell level. In five of the six patients, the subclone structure identified in the WES data was confirmed by the long-read scRNA-seq data (Fig. 4; Supplemental Figs. 5 and 6). We illustrate such concordance in patient 1, where the WES data showed a linear pattern of subclonal evolution (Fig. 4A). To visualize this same pattern of evolution within the scRNA-seq samples, we created a genotype matrix plot showing each cell's genotype at each somatic variant within the sample. Figure 4B presents the genotype matrix plot for the two samples from this patient, with 5% of cells in the pretreatment sample and 11% of cells in the relapse sample confidently assigned

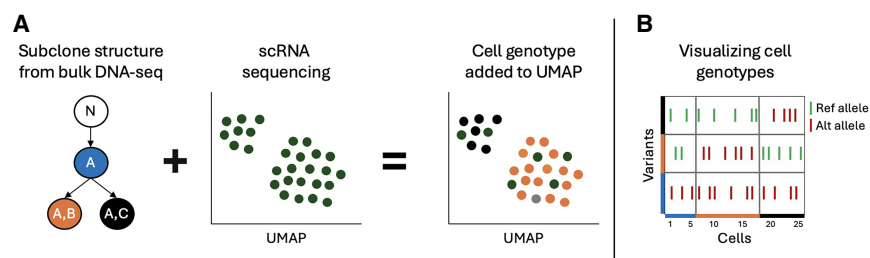


Figure 3. Overview of workflow to identify and use cell genotypes. (A) Predetermined subclone structures with accompanying somatic variant information are used to genotype individual cells in scRNA-seq data. Cells are assigned to a predetermined subclone based on the presence or absence of subclone-defining mutations. Subclone assignments are then used to group cells of the same subclone to identify subclone-specific gene expression. (B) Genotype matrix plots visualize the genotypes of all cells at each variant of interest, showing green for reference allele, red for alternate allele, and white for no coverage.

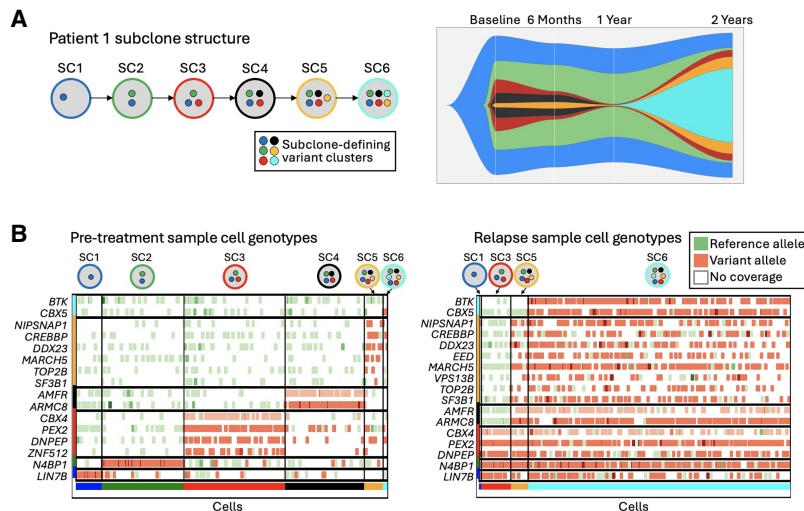


Figure 4. Visualization of single-cell genotypes to identify subclone structures. (A) The subclone structure of patient 1 was identified in the bulk DNA sequencing data. Subclones are depicted by the colored circles, with representative variant clusters inside each circle. The fishplot shows the prevalence of each subclone throughout treatment. (B) The cell genotypes at subclone-defining variants in patient 1. Each cell that was successfully assigned to a subclone is shown (x-axis), along with every somatic variant that was present in the WES data, labeled with the gene that the variant belongs to (y-axis). Green markers represent only reference alleles present in the scRNA-seq reads at the given variant location within the cell, and red markers indicate at least one scRNA-seq read in the cell contains the somatic variant allele. Darker marker coloring indicates an increased number of reads supporting that genotype. Variants and cells are grouped by their subclone assignment.

to a subclone. Cells belonging to the same subclone show similar genotype patterns, seen as clusters of red within the plot. The pre-treatment sample depicts five distinct subclones, each harboring the variants of the previous subclone. In the relapse sample, we again see the linear pattern of evolution where the *BTK*-mutated subclone (SC6) emerged and became the dominant subclone. By genotyping cells in the long-read scRNA-seq data, we conclude that the subclone structure identified through WES accurately represented the true subclonal heterogeneity in this patient's cancer.

For the remaining patient (patient 3, see Fig. 5), the resolution provided by long-read scRNA-seq highlighted the need to further refine the subclone structure that was previously constructed. In the WES of patient 3, two *BTK*^{C481S} mutations were identified at two different bases of the same codon (*BTK* c.1543T>A and *BTK* c.1544G>C), exhibiting similar VAFs in the samples where they were detected (Fig. 5A). Because VAFs are used to cluster variants and identify subclones in bulk DNA sequencing, these *BTK* mutations were initially clustered into the same subclone (SC2) alongside other variants with matching VAFs. We utilized the long-read scRNA-seq data to investigate individual cells with coverage at these *BTK* mutation sites and found that these two *BTK* mutations were, in fact, part of two distinct subclones. The genotype matrix plot for this patient's relapse sample reveals that among the 5% of confidently assigned cells, those with the *BTK* c.1544G>C mutation and its associated mutations never coexist with

the *BTK* c.1543T>A mutation (Fig. 5B). This increased resolution of the subclonal architecture afforded by the long-read scRNA-seq data allows us to conclude that rather than being on different haplotypes within the cells of a single subclone, these mutations belong to two distinct *BTK*-mutated subclones that had similar cellular prevalences in the patient sample (Fig. 5C).

Co-occurring CLL driver gene mutations are identified in *BTK*-mutated cells

Next, we wanted to determine whether cells with *BTK*^{C481S} mutations contained additional mutations in CLL driver genes. For this analysis, we genotyped *BTK*-mutated cells to identify the presence of mutated alleles in CLL driver genes. We found that the *BTK*-mutated subclones of all six patients contained additional mutations in driver genes at the time of relapse (Table 3). In all but one patient, these mutations were present in the cells before the *BTK* mutation developed and were detectable in the pre-treatment sample (Supplemental Fig. 5).

Patient 3, who had two independent *BTK*-mutated subclones emerge with similar allele frequencies, was the exception. When each of the *BTK*-mutated subclones developed in this patient, neither had any additional CLL-associated mutations that were detectable (Supplemental Fig. 6). One of these subclones continued to evolve, developing a mutation in *DICER1*—a gene recently implicated in CLL (Knisbacher et al. 2022). At the time of relapse, the *DICER1* and *BTK* co-mutated subclone demonstrated a higher prevalence in the sample compared to the *BTK*-only subclone.

Patient 5 also developed two independent *BTK*-mutated subclones during treatment (Supplemental Fig. 6). The first to develop did not harbor any additional CLL mutations. However, the

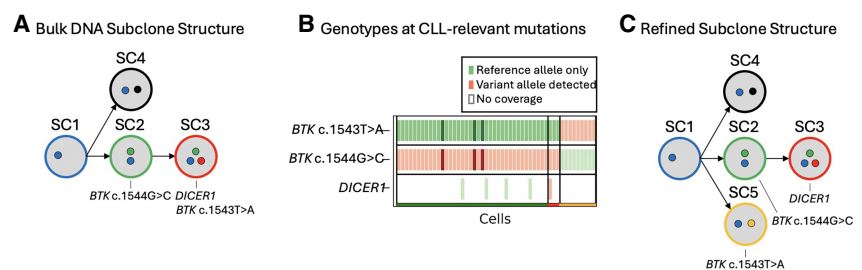


Figure 5. Refining the subclone structure of patient 3. (A) The subclone structure identified in the bulk DNA sequencing data of patient 3. CLL-relevant gene mutations are annotated under the subclone they are found in. (B) The genotype matrix plot from the relapse sample of patient 3 enables refinement of the original subclone structure. Each cell that was successfully assigned to a subclone is shown (x-axis), along with every CLL-relevant variant that was present in the WES data (y-axis). Green markers indicate that only reference alleles were present in the scRNA-seq reads at the given variant location within the cell, and red markers indicate that at least one scRNA-seq read in the cell contains the somatic variant allele. Darker coloring indicates an increased number of reads supporting that genotype. Only the CLL-relevant mutations are included for increased resolution to differentiate subclones. (C) The refined subclone structure that depicts the subclone containing the *BTK* c.1543T>A mutation is independent of the subclone containing the *BTK* c.1544G>C and *DICER1* mutations.

Table 3. The co-occurrence of mutations in CLL driver genes in *BTK*-mutated subclones

Patient ID	CLL mutations co-occurring with <i>BTK</i> ^{C481S}	CLL mutations were present before <i>BTK</i> ^{C481S} developed	<i>BTK</i> -mutated subclone was dominant subclone at relapse
1	<i>ASXL1</i> , <i>SF3B1</i> , <i>KMT2D</i> , <i>CREBBP</i>	Yes	Yes
2	<i>BRAF</i> , <i>SAMHD1</i> , <i>BCOR</i> , <i>NFKBIE</i> , <i>EGR2</i>	Yes	Yes
3	<i>DICER1</i>	No	Yes
4	<i>TP53</i>	Yes	No
5	<i>NOTCH1</i>	Yes	Yes
6	<i>SF3B1</i> , <i>POT1</i>	Yes	No

second *BTK*-mutated subclone arose from a cell population containing a *NOTCH1* mutation, a known CLL driver gene (Fabbri et al. 2011; Arruga et al. 2014). This second *BTK*-mutated subclone rapidly expanded and became the dominant subclone in the relapse sample.

Subclone assignments enabled by long-read scRNA-seq reveal transcriptomically distinct subclones

Utilizing the cell barcodes from the scBayes subclone assignments, we overlaid subclone identities onto gene expression-based cell clusters, facilitating inter-subclone gene expression comparisons. In the relapse sample of patient 1, we identified two distinct gene expression clusters. Mapping subclone assignments onto these clusters revealed that the larger cluster was primarily composed of cells from the *BTK*-mutated subclone, which had emerged as the dominant clone in that sample (Fig. 6A). The smaller cluster consisted of cells from the earlier original clone, highlighting the transcriptional divergence between these two populations. Of the six patients, patient 1 was the only case where the *BTK*-mutated subclone created a distinct cluster of cells within the transcriptomic data (Supplemental Fig. 7).

Differential gene expression analysis between the two clusters in patient 1 identified differential expression in seven genes that are either CLL driver genes or part of the BCR pathway (Fig. 6B; Supplemental Table S2). *IGLL5*, a gene implicated in CLL (Kasar et al. 2015; Pérez-Carretero et al. 2020; Deng et al. 2023), was overexpressed in the *BTK*-mutated subclone when compared to the original clone (Fig. 6C). *CD79A* and *CD79B*, two genes upstream of *BTK* in the BCR pathway, had lower levels of expression in the *BTK*-mutated subclone when compared to the original clone. These findings highlight the dual utility of long-read scRNA-seq in elucidating both genomic and transcriptomic subclonal dynamics within a single assay.

To demonstrate the utility of long-read scRNA-seq in identifying and classifying isoforms, we repeated the single-cell analysis using the isoform count matrix generated from the Iso-Seq pipeline. Mapping subclone identities onto the cells revealed the same distinct subclonal populations—the *BTK*-mutated subclone and the original clone—as observed in the gene expression analysis (Fig. 7A; Supplemental Fig. 9). Increased expression of two distinct *IGLL5* isoforms was observed in the *BTK*-mutated subclone, consistent with the findings from the gene expression analysis (Fig. 7B; Supplemental Table S2). No significant differential isoform usage was detected between these two clonal populations. The ability of long-read scRNA-seq to quantify isoform expression provides a more detailed understanding of gene expression at the isoform level.

To investigate treatment-induced transcriptional changes within individual subclones, we performed differential gene expression analysis between pretreatment and relapse samples for each subclone in patient 1 (Supplemental Fig. 8). This analysis was possible for Subclones 1, 3, and 5, which had assigned cells at both time points (Supplemental Table S3). Although we identified several differentially expressed genes, these changes did not explain the transcriptional differences previously observed between subclones. Among CLL and BCR pathway-associated genes, subclone 1 showed increased expression of *FOS* at relapse (adj. $P < 0.001$), whereas subclone 5 exhibited elevated *BIRC3* expression (adj. $P < 0.001$). No significant changes in genes related to CLL or the BCR pathway were detected in subclone 3. These analyses demonstrate the capability of long-read scRNA-seq to provide longitudinal intra-subclone analysis in addition to inter-subclone analysis.

Discussion

This study utilizes MAS-seq, PacBio's long-read scRNA-seq technology, to comprehensively analyze the subclonal dynamics and gene expression patterns within CLL, offering insights into the cellular heterogeneity and mechanisms underlying BTK inhibitor treatment resistance. This technological advancement represents an improvement over short-read scRNA-seq, primarily by improving on its limitations in transcript coverage and mutation site resolution. By comparing samples sequenced on the Sequel II and Revio instruments, we see a significant improvement in the quantity of data provided by the latter. When comparing to samples sequenced using traditional short-read scRNA-seq, we see increased transcript and variant coverage provided by MAS-seq.

Despite these improvements, much of our MAS-seq data is limited by the number of reads assigned to each cell. A scarcity of reads within a cell results in a lack of coverage for variants of interest, hindering the ability to assign that cell to a subclone. This limitation in variant coverage can be further exacerbated by technical factors such as allelic dropout or by biological factors like lower expression of genes of interest, which may receive fewer sequencing reads compared to highly expressed genes. Additionally, limited read coverage per cell restricts the ability to detect copy number events in single-cell populations, which could be valuable for informing subclone assignments. To address these limitations, strategies like CRISPR-Cas9-mediated depletion of over-represented cDNAs, e.g., those belonging to long-noncoding RNA, can be implemented to enhance the proportion of informative reads (Pandey et al. 2022; Wang and Adler 2023). Alternatively, targeted

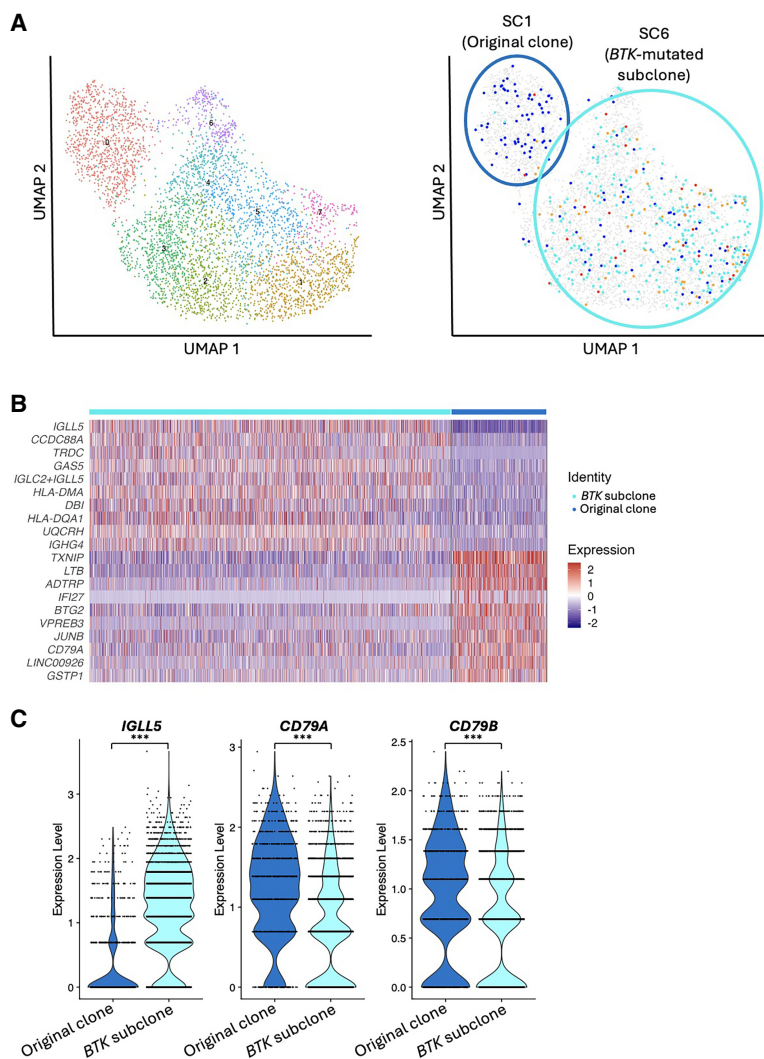


Figure 6. Using cell assignments to identify subclone-specific gene expression patterns. The results shown are from patient 1, who had a linear pattern of subclonal evolution with a *BTK* mutation present in the final subclone. The pattern of subclonal evolution and genotype matrix plot for this patient are depicted in Figure 4. (A) Mapping subclone assignments to clustered cells enables the identification of phenotypically distinct subclones. (B) Heatmap of differentially expressed genes between the Original clone and the *BTK*-mutated subclone. The top 10 upregulated genes in each clone are shown. (C) Differential gene expression analysis between subclones illuminates overexpressed and underexpressed genes within the *BTK*-mutated subclone. (***) adjusted P -value < 0.001.

enrichment strategies, such as hybridization capture for gene panels, could be utilized to enhance the read coverage in genes of interest (Pokhilko et al. 2021). By increasing the number of reads aligning to informative genes, these approaches would enable the detection of more variants and improve cell genotyping and gene expression analysis.

Our approach provides a framework for utilizing long-read scRNA-seq to investigate subclonal evolution on a single-cell level within a patient sample. When used in conjunction with bulk DNA-seq data, subclones can be identified and refined with greater resolution than using bulk DNA-seq alone. In one patient, we found that the data provided by the bulk DNA-seq was insufficient to identify the correct subclone structure due to two different subclones having very similar cellular prevalences. By investigating the genotypes within the cells of these subclones, we could deter-

mine that they were two independent subclones and improve the subclone structure.

When investigating the transcriptomic behavior within each patient, we identified one where the *BTK*-mutated subclone represents the cells of a distinct gene expression cluster. This separation enabled an inter-subclone differential gene expression analysis to identify genes that were overexpressed or underexpressed in the *BTK*-mutated subclone. No other patients showed the same pattern of *BTK*-mutated subclones being responsible for an isolated cluster within the transcriptomic data. Although informative, this analysis was limited by the number of reads per gene, restricting our ability to identify patterns of gene expression across more samples. This limitation is magnified when analyzing isoform expression and usage due to the spread of reads across more features. The high-quality data in the patient showing separation was a result of these samples being sequenced on the Revo instrument and benefiting from higher sample quality. This higher-quality data enabled a more robust analysis, clearly revealing the separation in gene expression across subclones. Increasing the number of reads per cell would allow for a more robust transcriptomic analysis within these cell populations and across more patients. To improve the quantification of gene expression while maintaining the additional information provided by long-read scRNA-seq, sequencing libraries could also be sequenced using a short-read technology to increase the number of reads per gene (Mincarelli et al. 2023; Torre et al. 2023). Although these reads would not provide the same full-transcript coverage, they would enable a higher-resolution gene expression analysis within the sample.

Two of the six patients included in this study developed two independent *BTK*-mutated subclones. In both cases, we observed that subclones harboring additional mutations in CLL driver genes, alongside the *BTK*^{C481S} mutation, exhibited greater expansion at the time of relapse compared to those without these additional driver mutations. Although our findings are limited by the small sample size, they suggest that the co-occurrence of these mutations may confer a survival advantage and contribute to therapy resistance, warranting further investigation.

Though we did not test whether gene expression alone can predict clonality, our findings suggest that combining gene expression data with DNA and RNA variant information provides a more comprehensive understanding of clonal structures within patients. Investigating the genotype and phenotype of *BTK*-mutated subclones in patients treated with *BTK* inhibitors can provide

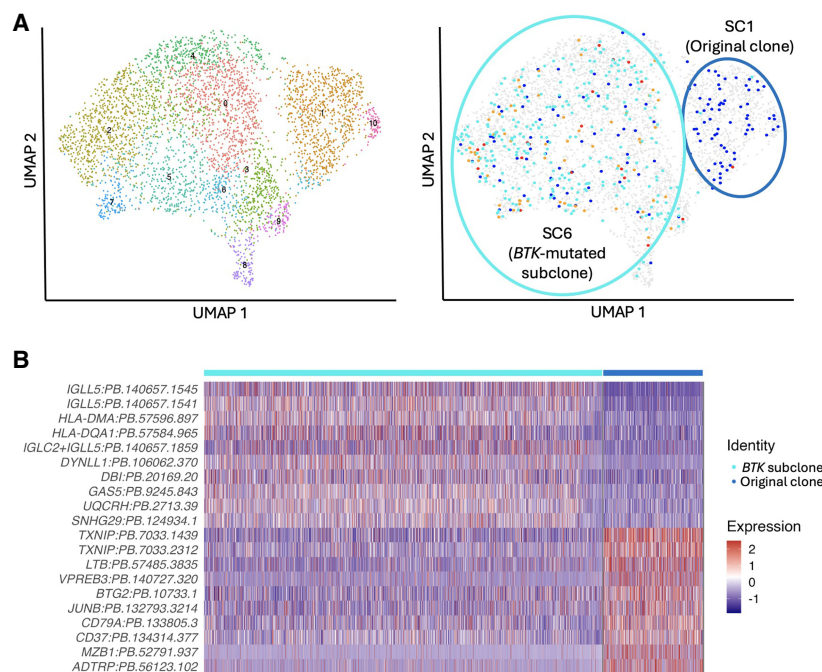


Figure 7. Using isoform expression analysis to complement gene expression analysis. The isoform expression analysis of the relapse sample of patient 1. (A) UMAP showing the isoform clustering. Mapping subclone assignments to clustered cells enables the identification of the same distinct clones identified in the gene expression analysis. (B) Heatmap showing differentially expressed isoforms between the Original clone and the *BTK*-mutated subclone. The top 10 upregulated isoforms for each clone are shown.

valuable insight into the mechanisms of clinical relapse and may aid in determining how quickly relapse will occur. Understanding subclonal evolution can help detect resistant clones early and guide specific subclone-directed therapy to reduce further selection of aggressive subclones. Combination therapy may be required to treat CLL with multiple subclones. Alternatively, the presence of multiple subclones may result in a clinical indication to shift to alternate therapies with distinct mechanisms of action from the current therapy.

Methods

CLL patient cohort

We received samples from six CLL patients treated with BTK inhibitors at The Ohio State University to undergo long-read scRNA-seq. Blood samples and other standard clinical data were collected through an IRB-approved tissue procurement protocol during routine clinical visits.

B cell isolation and library preparation

Peripheral blood mononuclear cells (PBMCs) were initially isolated from whole blood using ficoll density gradient centrifugation. PBMCs were then viably frozen. Prior to sequencing, samples were processed by sequentially using the EasySep Dead Cell Removal (Annexin V) Kit (cat # 17899), followed by buffer exchange and B cell selection using the EasySep Human B Cell Enrichment Kit II Without CD43 Depletion (cat # 17963) from Stemcell Technologies (Vancouver, BC). Following B cell selection, the 10x Genomics Chromium Next GEM Single Cell 3' Reagent Kits

v3.1 (Dual Index) was used for cell barcoding and cDNA generation. The standard protocol was followed until the end of step 2, stopping before cDNA cleavage. The resulting cDNA was used as input for the MAS-seq for 10x Single Cell 3' kit by PacBio.

Long-read sequencing and data processing

Four samples (pretreatment and relapse samples from patients 3 and 4) were sequenced on the PacBio Sequel II system using 8M SMRTCells for 30 h. The remaining samples were sequenced on the PacBio Revio system using Revio SMRT Cells for 24 h. Raw HiFi reads were segmented into representative cDNAs with SMRT Link v12.0.0.177059 using the 10x Genomics Chromium single cell 3' cDNA primers barcode set and MAS-seq Adapter v1 (MAS16) barcode set. We used PacBio's Iso-Seq single-cell workflow to trim, tag, and align reads using the default parameters of the tools distributed via Bioconda (<https://github.com/PacificBiosciences/pbbioconda>). Briefly, Lima v2.7.1 removed primers from the segmented reads. Iso-Seq v4.0.0 added tags for unique molecular identifiers (UMIs) and barcodes, followed by trimming of the poly(A) and primer sequences. Iso-Seq was then used to correct cell barcodes and deduplicate reads. Finally, pbmm2 v1.10.0 aligned reads to the reference genome using the GRCh38 reference sequence.

Reconstructing subclone structures from WES data

In a previous study, we collected 200× WES data for each patient at multiple time points throughout their treatment (Black et al. 2022, Supplemental Table S4, obtained from the database of Genotypes and Phenotypes (dbGaP; <https://www.ncbi.nlm.nih.gov/gap/>) under accession number phs003042.v1.p1). Reads were aligned to the GRCh38 reference genome with BWA-MEM v0.7.17 (Li and Durbin 2009). SAMBLASTER (Faust and Hall 2014) removed duplicate reads from the output generated by the alignment. SAMtools v1.16 (Li et al. 2009) was used to merge and sort BAM files by leftmost coordinates. All data processing commands were run using the default parameters for each tool.

We used FreeBayes v1.3.4 (Garrison and Marth 2012) to call variants within each patient. A minimum alternate fraction filter of 0.5 was used along with the following options: allele-balance-priors-off, report-genotype-likelihood-max, genotype-qualities, pooled-discrete, and pooled-continuous. The VCF that was generated from this script represents all variants within the patient and their allele count at each time point during BTK inhibitor treatment. Using BEDTools intersect v2.28.0 (Quinlan and Hall 2010), we removed any variants that did not fall within exonic regions or accessible regions specified by the 1000 Genomes Project (The 1000 Genomes Project Consortium 2015). Using SnpSift filter v4.3 (Cingolani et al. 2012), we filtered out variants with a quality score ≤ 20 or a sample depth of 50 or less. Only biallelic variants were used in our analysis. To filter for somatic variants, we used SnpSift filter to remove any variants that had more than five alternate allele observations in the germline sample. Copy number

variants were called using the FACETS v0.6.2 R package (Shen and Seshan 2016). Somatic variants found within copy number regions were excluded from the subclone analysis.

To identify subclones within the longitudinal data, we used PyClone-VI v0.1.1 (Gillis and Roth 2020) to cluster the somatic mutations identified in each patient. We ran `pyclone-vi fit` using the β -binomial model, 100 restarts, and a maximum of 10 clusters and added each variant's cluster assignment to its VCF info field. We reconstructed the subclonal architecture of the samples based on this clustering information using SuperSeeker (Qiao et al. 2014). Because many cells do not have coverage at subclone-defining mutation sites, we used passenger mutation information to impute subclone assignments based on VAFs that match the subclone-defining mutations, resulting in more cells being successfully assigned. A representation of the subclone structure was added as a header line to the somatic VCF file for downstream analysis.

Cell genotyping and assignment

Using the WES VCF file annotated with variant cluster identities and the subclonal structure, cells were genotyped and assigned to subclones using `scBayes v1.0.0` (Qiao et al. 2024). Aligned BAMs containing the long-read scRNA-seq reads for each sample and the VCF file containing the subclone annotations for the given patient were used as input for `scBayes`. First, we used `scGenotype` to create a matrix representing the genotype of each cell at all variant positions contained within the VCF file, with one row per variant and one column per cell barcode. `scAssign` was then used to assign each cell to a subclone based on the presence or absence of subclone-defining mutations in the genotype matrix. We used default parameters for each of these commands.

Genotype visualization

To visualize the cell genotypes across all cells in the sample, we developed a method that leverages the genotype matrix and cell assignment from `scBayes` to produce a genotype matrix plot. Within this scatterplot-like visualization framework, each cell is represented on the x -axis, with the variants of interest along the y -axis. Cell genotypes at these mutation sites are indicated with a marker: a green marker for cells with only reference alleles at the variant position, a red marker signifying the presence of at least one alternate allele, and no marker present when there is a lack of coverage at the variant position within the given cell. The organization of cells and variants within the plot is done by subclone assignment, enabling a visual depiction of the subclone structure embedded in the genomic data. Within each subclone, cells can be sorted by total read count, number of alternate variants, or assignment quality. By providing a list of disease-driving variants, plots can be tailored to include only cells with these variants to further identify co-occurring driver mutations. This approach takes into account variability in detection sensitivity, which may arise from differences in gene expression or limited read coverage across genes in each cell. We acknowledge that if all genes were expressed in each cell with complete read coverage, we would expect cells in certain subclones (e.g., SC3) to contain all variants found in other subclones (e.g., SC1, SC2, and SC3 in Fig. 4). However, as it is likely not all genes are expressed in every cell and read coverage remains limited on a per-cell level, this can affect the resolution of variant detection in our study. This comprehensive visualization approach offers greater insights into the subclonal architecture revealed by long-read scRNA-seq data.

Coverage metrics

We calculated the percentage of coverage each sequencing read provides to its given transcript by selecting all protein-coding

genes annotated in GENCODE v44 (Frankish et al. 2021) for calculation. For each protein-coding gene, we used `Pysam` to fetch reads that overlapped the genic region, only selecting reads where at least 90% of the read mapped between the gene's start and end position. Next, we calculated the exonic length of the canonical transcript as annotated by Ensembl (Martin et al. 2023) and determined what percentage of the canonical transcript was covered by a given read. Using these calculations, we determined the percentage of reads that covered X percent of the given transcript for each sample.

In addition, we calculated the fraction of heterozygous germline variants within the WES data that had read coverage within each cell. Variants were called using `FreeBayes` and filtered to only include variants present in all samples of the patient with a VAF between 30% and 70%. Using `scBayes`, we generated a genotype matrix for the germline variants using the `scGenotype` command. For each variant row in the matrix, we computed the number of cells containing any read that overlapped the variant position, as well as the number of cells with at least one read containing the given variant. The number of cells with variant coverage was divided by the total number of cells present in the sample to determine the percentage of cells covering that variant for plotting.

Transcriptomic analysis

`Seurat v4.3.0.1` (Hao et al. 2021) was used to cluster cells by gene expression and perform differential gene expression analysis. A count matrix of filtered, high-quality cells was generated using the `PacBio Iso-Seq` pipeline, which produces `Seurat-compatible` files for downstream transcriptomic analysis. The pipeline includes QC steps to filter for high-quality cells: mitochondrial DNA reads are removed during the `pigeon filter` step (`Pigeon v1.2.0`), and the `knee` method in the `iseq-correct` step quantifies UMIs per barcode to identify and retain only real cells. These steps occur before the count matrix is created, ensuring that the data loaded into `Seurat` contains only high-quality cells, rendering further mitochondrial or UMI-based filtering in `Seurat` redundant.

The `scTransform` method (Lause et al. 2021) was used to normalize raw gene counts and minimize technical variability. The standard `Seurat` workflow was applied as follows: `ScaleData()` and `RunPCA()` for dimensionality reduction, `RunUMAP()`, `FindNeighbors()`, and `FindClusters()` for unsupervised clustering. Dimensions 1 through 20 were selected for clustering and UMAP visualization, following the guidance from the `scTransform` vignette, which suggests that increasing the number of dimensions can enhance the benefits of normalization. The default cluster resolution of 0.8 was used, as it effectively identified the primary groups within subclones detected by `scBayes`, aligning with the focus of our analysis.

Subclone assignments were mapped onto cells using the UMAP coordinates of each cell barcode, enabling the identification of subclonal populations within clusters. Inter-subclone differential gene expression analysis was performed on clusters with subclone assignments using the `FindMarkers` function with the Wilcoxon rank sum test. P -values are adjusted using the Bonferroni correction. Tables with all fold change values with corresponding unadjusted and adjusted P -values for each differential gene expression analysis are included in the supplement. This approach was repeated using the isoform count matrix provided by `Pigeon` in the `Iso-Seq` pipeline to investigate differential isoform expression and usage between subclones within samples.

Software availability

The custom scripts and processed data sets generated and/or analyzed in the study are available at GitHub (<https://github.com/>)

gageblack/BTK-subclones) and as Supplemental Code. The Super-Seeker pipeline, used for the WES data analysis, is available at GitHub (https://github.com/gageblack/superseeker_pipeline) and as Supplemental Code.

Data access

The single-cell expression data generated in this study have been submitted to the NCBI Gene Expression Omnibus (GEO; <https://www.ncbi.nlm.nih.gov/geo/>) under accession number GSE259253.

Competing interest statement

D.M.S. has received research funding from Abbvie, AstraZeneca, Genentech, and Novartis and is a consultant for Abbvie, AstraZeneca, Beigene, Celgene, Eli Lilly, Genentech, Janssen, and Pharmacyclics. J.A.W. has received research funding from Abbvie, Janssen, Pharmacyclics, and Schrödinger and is a consultant for Abbvie, AstraZeneca, Beigene, Genentech, Janssen, Loxo/Lilly, Merck, Newave, and Pharmacyclics. The remaining authors declare no competing financial interests.

Acknowledgments

G.S.B., X.H., Y.Q., and G.T.M. were supported by National Institutes of Health (NIH) grant nos. U24CA209999 and U25CA224076-05. G.T.M. is a H.A. and Edna Benning Presidential Endowed Chair. D.M.S. is funded by the National Institute of Health, National Cancer Institute R50CA275929. J.A.W. is a clinical scholar of the Leukemia and Lymphoma Society. Research reported in this publication utilized the High-Throughput Genomics and Bioinformatic Analysis Shared Resource at Huntsman Cancer Institute at the University of Utah and was supported by the National Cancer Institute of the National Institutes of Health under award number P30 CA042014. The support and resources from the Center for High-Performance Computing at the University of Utah are gratefully acknowledged. The NIH Shared Instrumentation grant no. 1S10OD021644-01A1 partially funded the computational resources used for this study. We are grateful to the patients who provided tissue samples for these studies to the OSU Comprehensive Cancer Center Leukemia Tissue Bank Shared Resource (supported by NCI P30 CA016058). We also thank the OSU Leukemia Tissue Bank for assistance with the CLL samples. The content is solely the responsibility of the authors and does not necessarily represent the official views of the National Institutes of Health.

Author contributions: G.S.B., X.H., Y.Q., D.S., D.M.S., J.A.W., and G.T.M. conceived and designed the project. D.M.S. and J.A.W. contributed to the project coordination, clinical oversight, and sample collection and transfer. P.M. performed the sample preparation for long-read scRNA-seq. G.S.B. performed the data processing of the genomic and long-read scRNA-seq data, performed the subclone and gene expression analysis, and interpreted the results. X.H., Y.Q., and G.T.M. contributed to the analysis design and assisted in data analysis and the interpretation of results. G.S.B. wrote the manuscript with significant contributions from X.H., Y.Q., and G.T.M. All authors contributed to manuscript editing and refinement.

References

The 1000 Genomes Project Consortium. 2015. A global reference for human genetic variation. *Nature* **526**: 68–74. doi:10.1038/nature15393

- Al'Khafaji AM, Smith JT, Garimella KV, Babadi M, Popic V, Sade-Feldman M, Gatzen M, Sarkizova S, Schwartz MA, Blaum EM, et al. 2024. High-throughput RNA isoform sequencing using programmed cDNA concatenation. *Nat Biotechnol* **2**: 582–586. doi:10.1038/s41587-023-01815-7
- Arruga F, Gizdic B, Serra S, Vaisitti T, Ciardullo C, Coscia M, Laurenti L, D'Arena G, Jaksic O, Inghirami G, et al. 2014. Functional impact of NOTCH1 mutations in chronic lymphocytic leukemia. *Leukemia* **28**: 1060–1070. doi:10.1038/leu.2013.319
- Black GS, Huang X, Qiao Y, Tarapcsak S, Rogers KA, Misra S, Byrd JC, Marth GT, Stephens DM, Woyach JA. 2022. Subclonal evolution of CLL driver mutations is associated with relapse in ibrutinib- and acalabrutinib-treated patients. *Blood* **140**: 401–405. doi:10.1182/blood.2021015132
- Brady SW, McQuerry JA, Qiao Y, Piccolo SR, Shrestha G, Jenkins DF, Layer RM, Pedersen BS, Miller RH, Esch A, et al. 2017. Combating subclonal evolution of resistant cancer phenotypes. *Nat Commun* **8**: 1231. doi:10.1038/s41467-017-01174-3
- Burger JA, Chiorazzi N. 2013. B cell receptor signaling in chronic lymphocytic leukemia. *Trends Immunol* **34**: 592–601. doi:10.1016/j.it.2013.07.002
- Burger JA, Landau DA, Taylor-Weiner A, Bozic I, Zhang H, Sarosiek K, Wang L, Stewart C, Fan J, Hoellenriegel J, et al. 2016. Clonal evolution in patients with chronic lymphocytic leukaemia developing resistance to BTK inhibition. *Nat Commun* **7**: 11589. doi:10.1038/ncomms11589
- Byrd JC, Stilgenbauer S, Flinn IW. 2004. Chronic lymphocytic leukemia. *Hematology Am Soc Hematol Educ Program* **2004**: 163–183. doi:10.1182/asheducation-2004.1.163
- Byrd JC, Furman RR, Coutre SE, Flinn IW, Burger JA, Blum KA, Grant B, Sharman JP, Coleman M, Wierda WG, et al. 2013. Targeting BTK with ibrutinib in relapsed chronic lymphocytic leukemia. *N Engl J Med* **369**: 32–42. doi:10.1056/NEJMoa1215637
- Cingolani P, Patel VM, Coon M, Nguyen T, Land SJ, Ruden DM, Lu X. 2012. Using *Drosophila melanogaster* as a model for genotoxic mutational studies with a new program, SnpSift. *Front Genet* **3**: 35. doi:10.3389/fgene.2012.00035
- Deng X, Zhang M, Wang J, Zhou X, Xiao M. 2023. Characterization of clonal immunoglobulin heavy V-D-J gene rearrangements in Chinese patients with chronic lymphocytic leukemia: clinical features and molecular profiles. *Front Oncol* **13**: 1120867. doi:10.3389/fonc.2023.1120867
- Fabbri G, Rasi S, Rossi D, Trifonov V, Khiabanian H, Ma J, Grunn A, Fangazio M, Capello D, Monti S, et al. 2011. Analysis of the chronic lymphocytic leukemia coding genome: role of NOTCH1 mutational activation. *J Exp Med* **208**: 1389–1401. doi:10.1084/jem.20110921
- Faust GG, Hall IM. 2014. SAMBLASTER: fast duplicate marking and structural variant read extraction. *Bioinformatics* **30**: 2503–2505. doi:10.1093/bioinformatics/btu314
- Frankish A, Diekhans M, Jungreis I, Lagarde J, Loveland JE, Mudge JM, Sisu C, Wright JC, Armstrong J, Barnes I, et al. 2021. GENCODE 2021. *Nucleic Acids Res* **49**: D916–D923. doi:10.1093/nar/gkaa1087
- Garrison E, Marth G. 2012. Haplotype-based variant detection from short-read sequencing. arXiv:12073907 [q-bio]. <http://arxiv.org/abs/1207.3907> [accessed July 6, 2020] doi:10.48550/arXiv.1207.3907
- Gillis S, Roth A. 2020. PyClone-VI: scalable inference of clonal population structures using whole genome data. *BMC Bioinformatics* **21**: 571. doi:10.1186/s12859-020-03919-2
- Hao Y, Hao S, Andersen-Nissen E, Mauck WM III, Zheng S, Butler A, Lee MJ, Wilk AJ, Darby C, Zager M, et al. 2021. Integrated analysis of multimodal single-cell data. *Cell* **184**: 3573–3587.e29. doi:10.1016/j.cell.2021.04.048
- Herman SEM, Gordon AL, Hertlein E, Ramanunni A, Zhang X, Jaglowski S, Flynn J, Jones J, Blum KA, Buggy JJ, et al. 2011. Bruton tyrosine kinase represents a promising therapeutic target for treatment of chronic lymphocytic leukemia and is effectively targeted by PCI-32765. *Blood* **117**: 6287–6296. doi:10.1182/blood-2011-01-328484
- Huang X, Qiao Y, Brady SW, Factor RE, Downs-Kelly E, Farrell A, McQuerry JA, Shrestha G, Jenkins D, Johnson WE, et al. 2021. Novel temporal and spatial patterns of metastatic colonization from breast cancer rapid-autopsy tumor biopsies. *Genome Med* **13**: 170. doi:10.1186/s13073-021-00989-6
- Kasar S, Kim J, Improgo R, Tiao G, Polak P, Haradhvala N, Lawrence MS, Kiezun A, Fernandes SM, Bahl S, et al. 2015. Whole-genome sequencing reveals activation-induced cytidine deaminase signatures during indolent chronic lymphocytic leukaemia evolution. *Nat Commun* **6**: 8866. doi:10.1038/ncomms9866
- Kipps TJ, Stevenson FK, Wu CJ, Croce CM, Packham G, Wierda WG, O'Brien S, Gribben J, Rai K. 2017. Chronic lymphocytic leukaemia. *Nat Rev Dis Primers* **3**: 16096. doi:10.1038/nrdp.2016.96
- Knisbacher BA, Lin Z, Hahn CK, Gaiti F, Aran D, Burgos N, Caldas J, Cui J, Deshpande C, Du P, et al. 2022. Molecular map of chronic lymphocytic leukemia and its impact on outcome. *Nat Genet* **54**: 1664–1674. doi:10.1038/s41588-022-01140-w

- Komarova NL, Burger JA, Wodarz D. 2014. Evolution of ibrutinib resistance in chronic lymphocytic leukemia (CLL). *Proc Natl Acad Sci* **111**: 13906–13911. doi:10.1073/pnas.1409362111
- Landau DA, Tausch E, Taylor-Weiner AN, Stewart C, Reiter JG, Bahlo J, Kluth S, Bozic I, Lawrence M, Böttcher S, et al. 2015. Mutations driving CLL and their evolution in progression and relapse. *Nature* **526**: 525–530. doi:10.1038/nature15395
- Lause J, Berens P, Kobak D. 2021. Analytic Pearson residuals for normalization of single-cell RNA-seq UMI data. *Genome Biol* **22**: 258. doi:10.1186/s13059-021-02451-7
- Li H, Durbin R. 2009. Fast and accurate short read alignment with Burrows–Wheeler transform. *Bioinformatics* **25**: 1754–1760. doi:10.1093/bioinformatics/btp324
- Li H, Handsaker B, Wysoker A, Fennell T, Ruan J, Homer N, Marth G, Abecasis G, Durbin R, 1000 Genome Project Data Processing Subgroup. 2009. The Sequence Alignment/Map format and SAMtools. *Bioinformatics* **25**: 2078–2079. doi:10.1093/bioinformatics/btp352
- Martin FJ, Amode MR, Aneja A, Austine-Orimoloye O, Azov AG, Barnes I, Becker A, Bennett R, Berry A, Bhai J, et al. 2023. Ensembl 2023. *Nucleic Acids Res* **51**: D933–D941. doi:10.1093/nar/gkac958
- Mincarelli L, Uzun V, Wright D, Scoones A, Rushworth SA, Haerty W, Macaulay IC. 2023. Single-cell gene and isoform expression analysis reveals signatures of ageing in haematopoietic stem and progenitor cells. *Commun Biol* **6**: 558. doi:10.1038/s42003-023-04936-6
- Nakhoda S, Vistarop A, Wang YL. 2023. Resistance to Bruton tyrosine kinase inhibition in chronic lymphocytic leukaemia and non-Hodgkin lymphoma. *Br J Haematol* **200**: 137–149. doi:10.1111/bjh.18418
- Pal Singh S, Dammeijer F, Hendriks RW. 2018. Role of Bruton's tyrosine kinase in B cells and malignancies. *Mol Cancer* **17**: 57. doi:10.1186/s12943-018-0779-z
- Pandey AC, Bezney J, DeAscanis D, Kirsch E, Ahmed F, Crinklaw A, Choudhary KS, Mandala T, Deason J, Hamdi J, et al. 2022. A CRISPR-Cas9-based enhancement of high-throughput single-cell transcriptomics. bioRxiv doi:10.1101/2022.09.06.506867
- Pérez-Carretero C, Hernández-Sánchez M, González T, Quijada-Álamo M, Martín-Izquierdo M, Hernández-Sánchez J-M, Vidal M-J, de Coca AG, Aguilar C, Vargas-Pabón M, et al. 2020. Chronic lymphocytic leukemia patients with *IGH* translocations are characterized by a distinct genetic landscape with prognostic implications. *Int J Cancer* **147**: 2780–2792. doi:10.1002/ijc.33235
- Petro JB, Rahman SMJ, Ballard DW, Khan WN. 2000. Bruton's tyrosine kinase is required for activation of I κ b kinase and nuclear factor κ B in response to B cell receptor engagement. *J Exp Med* **191**: 1745–1754. doi:10.1084/jem.191.10.1745
- Pokhilko A, Handel AE, Curion F, Volpato V, Whiteley ES, Bøstrand S, Newey SE, Akerman CJ, Webber C, Clark MB, et al. 2021. Targeted single-cell RNA sequencing of transcription factors enhances the identification of cell types and trajectories. *Genome Res* **31**: 1069–1081. doi:10.1101/gr.273961.120
- Qiao Y, Quinlan AR, Jazaeri AA, Verhaak RGW, Wheeler DA, Marth GT. 2014. SubcloneSeeker: a computational framework for reconstructing tumor clone structure for cancer variant interpretation and prioritization. *Genome Biol* **15**: 443. doi:10.1186/s13059-014-0443-x
- Qiao Y, Huang X, Moos PJ, Ahmann JM, Pomictier AD, Deininger MW, Byrd JC, Woyach JA, Stephens DM, Marth GT. 2024. A Bayesian framework to study tumor subclone-specific expression by combining bulk DNA and single-cell RNA sequencing data. *Genome Res* **34**: 94–105. doi:10.1101/gr.278234.123
- Quinlan AR, Hall IM. 2010. BEDTools: a flexible suite of utilities for comparing genomic features. *Bioinformatics* **26**: 841–842. doi:10.1093/bioinformatics/btq033
- Sedlarikova L, Petrackova A, Papajik T, Turcsanyi P, Kriegova E. 2020. Resistance-associated mutations in chronic lymphocytic leukemia patients treated with novel agents. *Front Oncol* **10**: 894. doi:10.3389/fonc.2020.00894
- Shen R, Seshan VE. 2016. FACETS: allele-specific copy number and clonal heterogeneity analysis tool for high-throughput DNA sequencing. *Nucleic Acids Res* **44**: e131. doi:10.1093/nar/gkw520
- Than H, Qiao Y, Huang X, Yan D, Khorashad JS, Pomictier AD, Kovacovics TJ, Marth GT, O'Hare T, Deininger MW. 2018. Ongoing clonal evolution in chronic myelomonocytic leukemia on hypomethylating agents: a computational perspective. *Leukemia* **32**: 2049–2054. doi:10.1038/s41375-018-0050-z
- Torre D, Francoeur NJ, Kalma Y, Gross Carmel I, Melo BS, Deikus G, Allette K, Flohr R, Fridrikh M, Vlachos K, et al. 2023. Isoform-resolved transcriptome of the human preimplantation embryo. *Nat Commun* **14**: 6902. doi:10.1038/s41467-023-42558-y
- Wang K-T, Adler CE. 2023. CRISPR-Cas9-based depletion of 16S ribosomal RNA improves library complexity of single-cell RNA-sequencing in planarians. *BMC Genomics* **24**: 625. doi:10.1186/s12864-023-09724-4
- Wenger AM, Peluso P, Rowell WJ, Chang P-C, Hall RJ, Concepcion GT, Ebler J, Functammasan A, Kolesnikov A, Olson ND, et al. 2019. Accurate circular consensus long-read sequencing improves variant detection and assembly of a human genome. *Nat Biotechnol* **37**: 1155–1162. doi:10.1038/s41587-019-0217-9
- Woyach JA, Ruppert AS, Guinn D, Lehman A, Blachly JS, Lozanski A, Heerema NA, Zhao W, Coleman J, Jones D, et al. 2017. *BTK*^{C481S}-mediated resistance to ibrutinib in chronic lymphocytic leukemia. *J Clin Oncol* **35**: 1437–1443. doi:10.1200/JCO.2016.70.2282
- Ziegenhain C, Vieth B, Parekh S, Reinius B, Guillaumet-Adkins A, Smets M, Leonhardt H, Heyn H, Hellmann I, Enard W. 2017. Comparative analysis of single-cell RNA sequencing methods. *Mol Cell* **65**: 631–643.e4. doi:10.1016/j.molcel.2017.01.023

Received March 15, 2024; accepted in revised form January 30, 2025.